International Journal of Development Mathematics Vol 3 Issue 2, 252–277

INTERNATIONAL JOURNAL OF DEVELOPMENT MATHEMATICS
ISSN: 3026-8656 (Print) | 3026-8699 (Online)
journal homepage: https://ijdm.org.ng/index.php/Journals

Age-Structured Compartmental Model for Cholera Transmission Dynamics and Control in Shendam Local Government Area, Plateau State, Nigeria

Justice J. Mamza[a*] and Shuaibu A. Abdullahi[b]

[a]Department of Mathematics and Statistics, School of Science, Federal Polytechnic N'yak-Shendam, Plateau State, Nigeria.
[b]Department of Mathematics, Faculty of Physical Sciences, Modibbo Adama University, Yola, Nigeria.

ARTICLE INFO

Article history:

Received 02 February 2026
Received in Revised 26 May 2026
Accepted 30 May 2026

Keywords

Cholera, Age-structured model, Basic reproduction number, Stability analysis, Sensitivity analysis, Numerical simulation.

MSC 2020 Subject classification: 92D30, 92D25, 34D20

Abstract

Cholera remains a significant public health concern in regions with inadequate water, sanitation, and hygiene facilities. This study develops and analyzes an age-structured cholera transmission model with environmental contamination to investigate the dynamics of the disease in Shendam Local Government Area, Plateau State, Nigeria. The model incorporates susceptible, infected, and recovered children and adults, together with an environmental bacterial reservoir. Fundamental qualitative properties of the model, including positivity and boundedness of solutions, were established. The basic reproduction number, R_0, was derived using the next-generation matrix method, and stability analysis showed that the disease-free equilibrium is globally asymptotically stable when $R_0 < 1$, while the endemic equilibrium is globally asymptotically stable when $R_0 > 1$. The model was calibrated using monthly cholera case data from January to December 2025

*Corresponding author Tel: +234 8038883659
Email address: justcejantik@fedpolynyakshendam.edu.ng
https://doi.org/10.62054/ijdm/0302.17

through a least-squares fitting procedure in MATLAB, yielding good agreement between observed and simulated data. Sensitivity analysis revealed that direct and environmental transmission rates, as well as bacterial shedding, are the most influential parameters driving disease persistence, whereas recovery, bacterial decay, and improved sanitation contribute significantly to disease reduction. Numerical simulations further demonstrated that enhanced environmental hygiene and treatment interventions substantially decrease infection prevalence. The findings highlight the critical role of environmental contamination in sustaining cholera transmission and underscore the importance of integrated control measures, including improved sanitation, safe water supply, environmental management, and effective treatment programmes, for sustainable cholera control.

1 Introduction

Cholera is an acute diarrhoeal disease caused by the bacterium *Vibrio cholerae*, primarily transmitted through the consumption of contaminated water or food. The disease remains a major public health concern, particularly in low and middle-income countries where access to safe water, sanitation, and healthcare services is inadequate (WHO, 2022). Clinical manifestations range from mild diarrhoea to severe dehydration, circulatory collapse, and death if prompt treatment is not provided. Despite advances in prevention and treatment, cholera continues to cause substantial morbidity and mortality worldwide.

Globally, cholera remains endemic in many regions, with recurrent outbreaks reported across Africa, Asia, and parts of the Middle East. The World Health Organization estimates that approximately 1.3–4.0 million cholera cases and between 21,000 and 143,000 deaths occur annually (WHO, 2024a). Recent reports indicate a resurgence of cholera outbreaks in several countries, with the African region accounting for a disproportionately high burden of reported cases and deaths (Africa CDC, 2025; WHO, 2026). These trends highlight the continuing threat posed by cholera and the need for effective disease control strategies.

Nigeria is among the countries that experience recurrent cholera outbreaks, particularly during the rainy season when flooding often compromises water quality and sanitation systems (NCDC, 2020). Several outbreaks have been recorded across the country in recent years, resulting in significant morbidity and mortality. Northern Nigeria remains especially vulnerable due to inadequate water, sanitation, and hygiene (WASH) infrastructure, population displacement, rapid urbanization, and environmental factors that facilitate disease transmission. In Plateau State, recurrent outbreaks have been associated with poor sanitation, unsafe water sources, seasonal flooding, and population mobility (Abubakar et al., 2016; Ali et al., 2015). Although no major outbreak was reported in Plateau State as of early 2025, communities such as Shendam Local Government Area remain susceptible because of their environmental and socioeconomic conditions.

The transmission dynamics of cholera are complex because they involve interactions be-

tween human hosts and environmental reservoirs contaminated with *Vibrio cholerae*. Infection may occur through direct human-to-human contact or indirectly through contaminated water sources (Codeço, 2001). Since environmental bacterial concentration plays a significant role in disease spread, mathematical models that incorporate environmental transmission have become valuable tools for understanding cholera epidemiology and evaluating intervention strategies.

Mathematical modelling has contributed substantially to the study of infectious disease dynamics by providing quantitative frameworks for analysing disease transmission, predicting outbreak behaviour, and assessing control measures (Heesterbeek et al., 2015; Keeling & Rohani, 2008). Numerous cholera models have been developed to investigate the effects of environmental transmission, vaccination, demographic processes, and intervention strategies (Cai et al., 2020; Cheng et al., 2023; Codeço, 2001; Finger et al., 2018; Hartley et al., 2006; Hove-Musekwa et al., 2011; Mukandavire et al., 2011; Mwasa & Tchuenche , 2011; Sun et al., 2017; Tien & Earn, 2010). However, many existing models assume homogeneous mixing of the population and do not adequately account for age-specific differences in susceptibility, exposure, recovery, and contact behaviour.

Age structure is an important determinant of disease transmission because children and adults often exhibit distinct behavioural patterns, exposure risks, and immune responses (Anderson & May, 1991; Hethcote, 2000). Previous studies have demonstrated that age-structured models provide more realistic descriptions of disease dynamics and can identify high-risk groups for targeted interventions (Cai et al., 2017; Cheng et al., 2024; Lin et al., 2019; Mossong et al., 2008; Wallinga et al., 2006; Yang et al., 2014). Although age-structured approaches have been applied to several infectious diseases, relatively few cholera studies explicitly distinguish between children and adults while simultaneously incorporating environmental transmission.

Motivated by the continued burden of cholera in Nigeria, this study develops and analyses an age-structured cholera transmission model for Shendam Local Government Area, Plateau State. The model incorporates child and adult populations, each stratified into susceptible, infectious, and recovered classes, together with an environmental reservoir of *Vibrio cholerae*, thereby capturing both demographic heterogeneity and environmental transmission dynamics. The model formulation, analytical results, parameter estimation, sensitivity analysis, and numerical simulations are presented in Sections 2 and 3, while the results, discussion, and conclusions are provided in Sections 4, 5, and 6, respectively.

2 Mathematical Model Formulation

The human population is stratified into susceptible, infected, and recovered classes for both children and adults, denoted by $S_c(t)$, $I_c(t)$, $R_c(t)$, $S_a(t)$, $I_a(t)$, and $R_a(t)$, respectively. An additional variable, $B(t)$, represents the concentration of *Vibrio cholerae* in the environment. The state variables, model parameters, and transmission dynamics are summarized in Table 1, Table 2, and Figure 1, respectively. The resulting cholera transmission dynamics are described by the following system of nonlinear differential

equations:

$$\begin{aligned}
\frac{dS_c}{dt} &= \Lambda + \omega_c R_c - \left(\beta_{cc} I_c + \frac{\beta_b B}{K+B} + \phi + \mu\right) S_c, \\
\frac{dS_a}{dt} &= \phi S_c + \omega_a R_a - \left(\beta_{aa} I_a + \frac{\beta_b B}{K+B} + \mu\right) S_a, \\
\frac{dI_c}{dt} &= \left(\beta_{cc} I_c + \frac{\beta_b B}{K+B}\right) S_c - (\gamma_c + \delta_c + \mu) I_c, \\
\frac{dI_a}{dt} &= \left(\beta_{aa} I_a + \frac{\beta_b B}{K+B}\right) S_a - (\gamma_a + \delta_a + \mu) I_a, \\
\frac{dR_c}{dt} &= \gamma_c I_c - (\omega_c + \mu) R_c, \\
\frac{dR_a}{dt} &= \gamma_a I_a - (\omega_a + \mu) R_a, \\
\frac{dB}{dt} &= \alpha_c I_c + \alpha_a I_a - (\theta + \mu_b) B.
\end{aligned} \tag{1}$$

The susceptible children population S_c increases through recruitment at rate Λ and through loss of immunity among recovered children at rate $\omega_c R_c$. The population decreases due to infection from infected children at rate $\beta_{cc} I_c S_c$, infection through contact with contaminated environment at rate $\frac{\beta_b B}{K+B} S_c$, progression into the adult susceptible class at rate ϕS_c, and natural death at rate μS_c.

The susceptible adult population S_a increases through maturation of susceptible children at rate ϕS_c and through waning immunity among recovered adults at rate $\omega_a R_a$. The adult susceptible class decreases through infection caused by infected adults at rate $\beta_{aa} I_a S_a$, environmental transmission at rate $\frac{\beta_b B}{K+B} S_a$, and natural mortality at rate μS_a.

The infected children compartment I_c increases when susceptible children acquire infection either through direct child-to-child transmission or through exposure to contaminated bacteria in the environment. Infected children leave the compartment through recovery at rate $\gamma_c I_c$, disease-induced death at rate $\delta_c I_c$, and natural death at rate μI_c.

Similarly, the infected adult compartment I_a increases through adult-to-adult transmission and environmental exposure, while infected adults recover at rate $\gamma_a I_a$, die due to disease at rate $\delta_a I_a$, or die naturally at rate μI_a.

Recovered children R_c are generated through recovery of infected children at rate $\gamma_c I_c$. Recovered children lose immunity at rate $\omega_c R_c$ and experience natural mortality at rate μR_c.

Recovered adults R_a arise from recovery of infected adults at rate $\gamma_a I_a$. They lose immunity at rate $\omega_a R_a$ and die naturally at rate μR_a.

The bacterial population B increases due to shedding of pathogens by infected children and infected adults at rates $\alpha_c I_c$ and $\alpha_a I_a$, respectively. The bacterial concentration decreases through environmental sanitation or cleaning at rate θB and natural bacterial decay at rate $\mu_b B$.

The term $\frac{\beta_b B}{K+B}$ is a saturated incidence function representing environmental transmission,

where K denotes the half-saturation constant. This formulation captures the nonlinear effect of bacterial concentration on disease transmission.

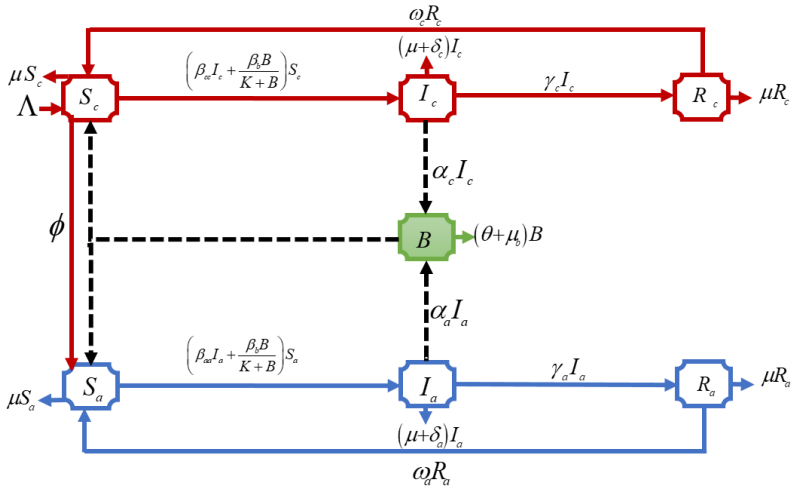

Figure 1. Schematic Diagram of the Model.

Table 1. Description of state variables

Variable	Description
$S_c(t)$	Population of susceptible children at time t
$S_a(t)$	Population of susceptible adults at time t
$I_c(t)$	Population of infected children at time t
$I_a(t)$	Population of infected adults at time t
$R_c(t)$	Population of recovered children at time t
$R_a(t)$	Population of recovered adults at time t
$B(t)$	Concentration of pathogenic bacteria in the environment at time t

Table 2. Description of model parameters

Parameter	Description
Λ	Recruitment rate into the susceptible children population
β_{cc}	Transmission rate from infected children to susceptible children
β_{aa}	Transmission rate from infected adults to susceptible adults
β_b	Environmental transmission rate due to contaminated bacteria
ϕ	Progression/maturation rate from children to adults
μ	Natural death rate of humans
γ_c	Recovery rate of infected children
γ_a	Recovery rate of infected adults
δ_c	Disease-induced death rate for infected children
δ_a	Disease-induced death rate for infected adults
ω_c	Loss of immunity rate for recovered children
ω_a	Loss of immunity rate for recovered adults
α_c	Bacterial shedding rate by infected children
α_a	Bacterial shedding rate by infected adults
θ	Bacterial removal rate due to environmental sanitation
μ_b	Natural death/decay rate of bacteria
K	Half-saturation constant for environmental transmission

3 Analysis of the Model

3.1 Positivity and Boundedness

3.1.1 Positivity of Solutions

In epidemiological modeling, it is important to show that all state variables remain nonnegative for all time since they represent human populations and bacterial concentration. We therefore establish the positivity of solutions of the model.

Theorem 3.1 (Positivity)**.** *Let*

$$(S_c(0), S_a(0), I_c(0), I_a(0), R_c(0), R_a(0), B(0)) \in \mathbb{R}^7_+.$$

Then all solutions of the model remain nonnegative for all $t > 0$. Hence, the nonnegative orthant

$$\mathbb{R}^7_+ = \left\{(S_c, S_a, I_c, I_a, R_c, R_a, B) \in \mathbb{R}^7 : S_c, S_a, I_c, I_a, R_c, R_a, B \geq 0\right\}$$

is positively invariant.

Proof. To establish positivity, suppose there exists a first time $t_1 > 0$ at which one of the state variables becomes zero while all variables remain positive on $[0, t_1)$. Evaluating

the corresponding model equation at $t = t_1$ gives

$$\left.\frac{dS_c}{dt}\right|_{t=t_1} = \Lambda + \omega_c R_c(t_1) > 0,$$

$$\left.\frac{dS_a}{dt}\right|_{t=t_1} = \phi S_c(t_1) + \omega_a R_a(t_1) \geq 0,$$

$$\left.\frac{dI_c}{dt}\right|_{t=t_1} = \frac{\beta_b B(t_1)}{K + B(t_1)} S_c(t_1) \geq 0,$$

$$\left.\frac{dI_a}{dt}\right|_{t=t_1} = \frac{\beta_b B(t_1)}{K + B(t_1)} S_a(t_1) \geq 0,$$

$$\left.\frac{dR_c}{dt}\right|_{t=t_1} = \gamma_c I_c(t_1) \geq 0,$$

$$\left.\frac{dR_a}{dt}\right|_{t=t_1} = \gamma_a I_a(t_1) \geq 0,$$

and

$$\left.\frac{dB}{dt}\right|_{t=t_1} = \alpha_c I_c(t_1) + \alpha_a I_a(t_1) \geq 0.$$

Thus, none of the state variables can cross the boundary of the nonnegative orthant into the negative region. Therefore, all solutions remain nonnegative for all $t > 0$, and the region $\mathbb{R}^7_+$ is positively invariant.

3.1.2 Boundedness of Solutions

In this section, we show that the solutions of the model remain bounded in a biologically meaningful feasible region. This guarantees that the population variables and bacterial concentration do not grow without bound as time increases.

Proposition 3.2 (Boundedness)**.** *All solutions of the model with nonnegative initial conditions remain nonnegative and bounded for all $t > 0$. Furthermore, the feasible region*

$$\Omega = \left\{ (S_c, S_a, I_c, I_a, R_c, R_a, B) \in \mathbb{R}^7_+ : N(t) \leq \frac{\Lambda}{\mu}, \quad B(t) \leq \frac{\Lambda(\alpha_c + \alpha_a)}{\mu(\theta + \mu_b)} \right\},$$

is positively invariant.

Proof. Let

$$N(t) = S_c + S_a + I_c + I_a + R_c + R_a.$$

Adding the first six equations of the model gives

$$\frac{dN}{dt} = \Lambda - \mu N - \delta_c I_c - \delta_a I_a.$$

Since $\delta_c I_c, \delta_a I_a \geq 0$, we obtain

$$\frac{dN}{dt} \leq \Lambda - \mu N.$$

Applying the Comparison Theorem in (Lakshmikantham & Leela, 1969) yields

$$N(t) \leq \frac{\Lambda}{\mu} + \left(N(0) - \frac{\Lambda}{\mu}\right) e^{-\mu t},$$

so that

$$0 \leq N(t) \leq \frac{\Lambda}{\mu} \qquad \text{for all } t > 0.$$

Similarly, from the bacterial population equation,

$$\frac{dB}{dt} = \alpha_c I_c + \alpha_a I_a - (\theta + \mu_b)B,$$

and using $I_c, I_a \leq N(t) \leq \Lambda/\mu$, we obtain

$$\frac{dB}{dt} \leq \frac{\Lambda(\alpha_c + \alpha_a)}{\mu} - (\theta + \mu_b)B.$$

Again, by the Comparison Theorem in (Lakshmikantham & Leela, 1969),

$$B(t) \leq \frac{\Lambda(\alpha_c + \alpha_a)}{\mu(\theta + \mu_b)} \qquad \text{as } t \to \infty.$$

Hence, all state variables remain bounded in Ω. Therefore, the feasible region Ω is positively invariant and biologically meaningful.

3.2 Disease-Free Equilibrium Point

The equilibrium points of the model are obtained by setting

$$\frac{dS_c}{dt} = \frac{dS_a}{dt} = \frac{dI_c}{dt} = \frac{dI_a}{dt} = \frac{dR_c}{dt} = \frac{dR_a}{dt} = \frac{dB}{dt} = 0.$$

At the disease-free equilibrium (DFE), there are no infected individuals and no bacterial concentration in the environment. Thus,

$$I_c = I_a = R_c = R_a = B = 0.$$

Substituting these conditions into the equilibrium equations gives

$$S_c^0 = \frac{\Lambda}{\phi + \mu}, \qquad S_a^0 = \frac{\phi\Lambda}{\mu(\phi + \mu)}.$$

Hence, the disease-free equilibrium point of the system is

$$E^0 = \left(\frac{\Lambda}{\phi + \mu}, \frac{\phi\Lambda}{\mu(\phi + \mu)}, 0, 0, 0, 0, 0\right).$$

3.3 Basic Reproduction Number

The basic reproduction number, denoted by R_0, is derived using the next-generation matrix method in (Diekmann et al., 2010; Driessche & Watmough , 2002). The Jacobian matrix associated with new infection terms evaluated at the DFE is

$$F = \begin{pmatrix} \beta_{cc}S_c^0 & 0 & \dfrac{\beta_b S_c^0}{K} \\ 0 & \beta_{aa}S_a^0 & \dfrac{\beta_b S_a^0}{K} \\ 0 & 0 & 0 \end{pmatrix},$$

while the transition matrix is

$$V = \begin{pmatrix} \gamma_c + \delta_c + \mu & 0 & 0 \\ 0 & \gamma_a + \delta_a + \mu & 0 \\ -\alpha_c & -\alpha_a & \theta + \mu_b \end{pmatrix}.$$

The inverse of V is given by

$$V^{-1} = \begin{pmatrix} \dfrac{1}{A_c} & 0 & 0 \\ 0 & \dfrac{1}{A_a} & 0 \\ \dfrac{\alpha_c}{A_c Q} & \dfrac{\alpha_a}{A_a Q} & \dfrac{1}{Q} \end{pmatrix},$$

where

$$A_c = \gamma_c + \delta_c + \mu, \qquad A_a = \gamma_a + \delta_a + \mu, \qquad Q = \theta + \mu_b.$$

Hence, the next-generation matrix becomes

$$FV^{-1} = \begin{pmatrix} \dfrac{\beta_{cc}S_c^0}{A_c} + \dfrac{\beta_b\alpha_c S_c^0}{KA_cQ} & \dfrac{\beta_b\alpha_a S_c^0}{KA_aQ} & \dfrac{\beta_b S_c^0}{KQ} \\ \dfrac{\beta_b\alpha_c S_a^0}{KA_cQ} & \dfrac{\beta_{aa}S_a^0}{A_a} + \dfrac{\beta_b\alpha_a S_a^0}{KA_aQ} & \dfrac{\beta_b S_a^0}{KQ} \\ 0 & 0 & 0 \end{pmatrix}.$$

The basic reproduction number is defined as the spectral radius of the next-generation matrix:

$$R_0 = \rho(FV^{-1}).$$

Thus,

$$R_0 = \max\{R_c, R_a\},$$

where

$$R_c = \frac{\beta_{cc}\Lambda}{(\phi+\mu)(\gamma_c+\delta_c+\mu)} + \frac{\beta_b\alpha_c\Lambda}{K(\phi+\mu)(\gamma_c+\delta_c+\mu)(\theta+\mu_b)},$$

and

$$R_a = \frac{\beta_{aa}\phi\Lambda}{\mu(\phi+\mu)(\gamma_a+\delta_a+\mu)} + \frac{\beta_b\alpha_a\phi\Lambda}{K\mu(\phi+\mu)(\gamma_a+\delta_a+\mu)(\theta+\mu_b)}.$$

Therefore, R_0 represents the average number of secondary infections generated by a single infectious individual introduced into a wholly susceptible population. Thus, the following lemma is established:

Lemma 3.3. *The disease-free equilibrium is locally asymptotically stable if* $R_0 < 1$, *and unstable if* $R_0 > 1$.

3.4 Existence of the Endemic Equilibrium Point

In this section, we establish the existence of the endemic equilibrium point (EEP) of the model. The endemic equilibrium corresponds to a steady-state solution at which the disease persists in the population, namely,

$$I_c^* > 0, \qquad I_a^* > 0, \qquad B^* > 0.$$

3.4.1 Equilibrium Equations

Let

$$E^* = (S_c^*, S_a^*, I_c^*, I_a^*, R_c^*, R_a^*, B^*)$$

denote an endemic equilibrium point of the system. Setting

$$\frac{dS_c}{dt} = \frac{dS_a}{dt} = \frac{dI_c}{dt} = \frac{dI_a}{dt} = \frac{dR_c}{dt} = \frac{dR_a}{dt} = \frac{dB}{dt} = 0,$$

we obtain the equilibrium system

$$\Lambda + \omega_c R_c^* - \left(\beta_{cc} I_c^* + \frac{\beta_b B^*}{K+B^*} + \phi + \mu\right) S_c^* = 0, \tag{2}$$

$$\phi S_c^* + \omega_a R_a^* - \left(\beta_{aa} I_a^* + \frac{\beta_b B^*}{K+B^*} + \mu\right) S_a^* = 0, \tag{3}$$

$$\left(\beta_{cc} I_c^* + \frac{\beta_b B^*}{K+B^*}\right) S_c^* = (\gamma_c + \delta_c + \mu) I_c^*, \tag{4}$$

$$\left(\beta_{aa} I_a^* + \frac{\beta_b B^*}{K+B^*}\right) S_a^* = (\gamma_a + \delta_a + \mu) I_a^*, \tag{5}$$

$$R_c^* = \frac{\gamma_c I_c^*}{\omega_c + \mu}, \tag{6}$$

$$R_a^* = \frac{\gamma_a I_a^*}{\omega_a + \mu}, \tag{7}$$

and

$$B^* = \frac{\alpha_c I_c^* + \alpha_a I_a^*}{\theta + \mu_b}. \tag{8}$$

Substituting equations (6)–(8) into equations (2) and (3) yields

$$S_c^* = \frac{\Lambda + \dfrac{\omega_c \gamma_c I_c^*}{\omega_c + \mu}}{\beta_{cc} I_c^* + \dfrac{\beta_b B^*}{K + B^*} + \phi + \mu}, \tag{9}$$

and

$$S_a^* = \frac{\phi S_c^* + \dfrac{\omega_a \gamma_a I_a^*}{\omega_a + \mu}}{\beta_{aa} I_a^* + \dfrac{\beta_b B^*}{K + B^*} + \mu}. \tag{10}$$

3.4.2 Existence of the Endemic Equilibrium

We now establish the existence of a positive endemic equilibrium.

Theorem 3.4. *Given that the feasible region*

$$\Omega = \left\{ (S_c, S_a, I_c, I_a, R_c, R_a, B) \in \mathbb{R}_+^7 : N(t) \leq \frac{\Lambda}{\mu}, \quad B(t) \leq \frac{\Lambda(\alpha_c + \alpha_a)}{\mu(\theta + \mu_b)} \right\},$$

is positively invariant. The model admits at least one endemic equilibrium point in Ω *whenever* $R_0 > 1$.

Proof. Define the forces of infection

$$\lambda_c^* = \beta_{cc} I_c^* + \frac{\beta_b B^*}{K + B^*},$$

and

$$\lambda_a^* = \beta_{aa} I_a^* + \frac{\beta_b B^*}{K + B^*}.$$

Using equations (9) and (10), we obtain

$$S_c^* = \frac{\Lambda(\omega_c + \mu) + \omega_c \gamma_c I_c^*}{(\omega_c + \mu)(\lambda_c^* + \phi + \mu)}, \tag{11}$$

and

$$S_a^* = \frac{\phi(\omega_a + \mu) S_c^* + \omega_a \gamma_a I_a^*}{(\omega_a + \mu)(\lambda_a^* + \mu)}. \tag{12}$$

Substituting equations (11) and (12) into equations (4) and (5) gives

$$\lambda_c^* \left(\frac{\Lambda(\omega_c + \mu) + \omega_c \gamma_c I_c^*}{(\omega_c + \mu)(\lambda_c^* + \phi + \mu)} \right) = (\gamma_c + \delta_c + \mu) I_c^*, \tag{13}$$

and

$$\lambda_a^* \left(\frac{\phi(\omega_a + \mu) S_c^* + \omega_a \gamma_a I_a^*}{(\omega_a + \mu)(\lambda_a^* + \mu)} \right) = (\gamma_a + \delta_a + \mu) I_a^*. \tag{14}$$

Furthermore, from equation (8),

$$B^* = \frac{\alpha_c I_c^* + \alpha_a I_a^*}{\theta + \mu_b}. \tag{15}$$

Equations (13)–(15) define a continuous nonlinear mapping

$$\mathcal{F} : \Omega \to \Omega.$$

Since the feasible region Ω is positively invariant and bounded, it follows that Ω is compact and convex in $\mathbb{R}_+^7$. Moreover, all model parameters are positive; hence the mapping $\mathcal{F}$ is continuous on Ω. Furthermore, when $R_0 > 1$, the disease-free equilibrium loses stability and the infection components satisfy $I_c^* > 0$, $I_a^* > 0$. Consequently, equations (13)–(15) admit positive solutions in Ω. Therefore, by Brouwer's Fixed Point Theorem in (Granas & Dugundji, 2003), the mapping $\mathcal{F}$ possesses at least one fixed point

$$E^* = (S_c^*, S_a^*, I_c^*, I_a^*, R_c^*, R_a^*, B^*) \in \Omega.$$

Finally, equations (6)–(8) imply that $R_c^* > 0$, $R_a^* > 0$, $B^* > 0$, whenever $I_c^* > 0$, $I_a^* > 0$. Similarly, equations (11) and (12) yield $S_c^* > 0$, $S_a^* > 0$. Hence, E^* is a positive endemic equilibrium point of the system whenever $R_0 > 1$. This completes the proof.

3.5 Stability Analysis

3.5.1 Global Stability Analysis of the Disease-Free Equilibrium

In this section, we establish the global asymptotic stability of the disease-free equilibrium (DFE) using the Lyapunov direct method together with LaSalle's Invariance Principle.

Theorem 3.5. *Given that the feasible region Ω is positively invariant. Then the disease-free equilibrium point E_0 is globally asymptotically stable in Ω whenever $R_0 < 1$.*

Proof.

Consider the Lyapunov function

$$V(I_c, I_a, B) = a_1 I_c + a_2 I_a + a_3 B, \tag{16}$$

where $a_1, a_2, a_3 > 0$ are constants to be determined.

Differentiating V along the trajectories of the system gives

$$\dot{V} = a_1 \dot{I}_c + a_2 \dot{I}_a + a_3 \dot{B}. \tag{17}$$

Substituting the model equations yields

$$\begin{aligned}\dot{V} =& a_1\left[\left(\beta_{cc}I_c+\frac{\beta_b B}{K+B}\right)S_c-(\gamma_c+\delta_c+\mu)I_c\right]\\ &+a_2\left[\left(\beta_{aa}I_a+\frac{\beta_b B}{K+B}\right)S_a-(\gamma_a+\delta_a+\mu)I_a\right]\\ &+a_3\left[\alpha_c I_c+\alpha_a I_a-(\theta+\mu_b)B\right].\end{aligned} \tag{18}$$

Since the feasible region Ω is positively invariant, we have $S_c \leq S_c^0, \quad S_a \leq S_a^0$.

Furthermore, since $\frac{B}{K+B} \leq \frac{B}{K}$, it follows that

$$\begin{aligned}\dot{V} \leq& a_1\left[\beta_{cc}S_c^0 I_c+\frac{\beta_b S_c^0}{K}B-(\gamma_c+\delta_c+\mu)I_c\right]\\ &+a_2\left[\beta_{aa}S_a^0 I_a+\frac{\beta_b S_a^0}{K}B-(\gamma_a+\delta_a+\mu)I_a\right]\\ &+a_3\left[\alpha_c I_c+\alpha_a I_a-(\theta+\mu_b)B\right].\end{aligned} \tag{19}$$

Rearranging terms gives

$$\begin{aligned}\dot{V} \leq& \left[a_1\beta_{cc}S_c^0-a_1(\gamma_c+\delta_c+\mu)+a_3\alpha_c\right]I_c\\ &+\left[a_2\beta_{aa}S_a^0-a_2(\gamma_a+\delta_a+\mu)+a_3\alpha_a\right]I_a\\ &+\left[\frac{a_1\beta_b S_c^0}{K}+\frac{a_2\beta_b S_a^0}{K}-a_3(\theta+\mu_b)\right]B.\end{aligned} \tag{20}$$

Choose $a_1=\frac{1}{\gamma_c+\delta_c+\mu}, \quad a_2=\frac{1}{\gamma_a+\delta_a+\mu}$, and $a_3=\frac{\beta_b}{K(\theta+\mu_b)}\left(\frac{S_c^0}{\gamma_c+\delta_c+\mu}+\frac{S_a^0}{\gamma_a+\delta_a+\mu}\right)$.

Substituting these choices into $\dot{V}$ gives

$$\begin{aligned}\dot{V} \leq& \left[\frac{\beta_{cc}S_c^0}{\gamma_c+\delta_c+\mu}+\frac{\beta_b\alpha_c S_c^0}{K(\gamma_c+\delta_c+\mu)(\theta+\mu_b)}-1\right]I_c\\ &+\left[\frac{\beta_{aa}S_a^0}{\gamma_a+\delta_a+\mu}+\frac{\beta_b\alpha_a S_a^0}{K(\gamma_a+\delta_a+\mu)(\theta+\mu_b)}-1\right]I_a.\end{aligned} \tag{21}$$

Using the expressions R_c and R_a we obtain

$$\dot{V} \leq (R_c-1)I_c+(R_a-1)I_a. \tag{22}$$

Since $R_0=\max\{R_c,R_a\}$, it follows that if $R_0<1$, then $R_c<1, \quad R_a<1$, and therefore, $\dot{V}\leq 0$. Moreover, $\dot{V}=0$ if and only if $I_c=0, \quad I_a=0$. Substituting $I_c=I_a=0$ into the bacterial equation gives

$$\frac{dB}{dt}=-(\theta+\mu_b)B,$$

which implies $B = 0$. Similarly,

$$\frac{dR_c}{dt} = -(\omega_c + \mu)R_c, \qquad \frac{dR_a}{dt} = -(\omega_a + \mu)R_a,$$

so that $R_c = R_a = 0$. The remaining subsystem becomes

$$\frac{dS_c}{dt} = \Lambda - (\phi + \mu)S_c, \qquad \frac{dS_a}{dt} = \phi S_c - \mu S_a,$$

whose unique equilibrium is $S_c = S_c^0, \quad S_a = S_a^0$. Hence, the largest invariant subset contained in $\{\dot{V} = 0\}$ is the singleton set $\{E_0\}$. Therefore, by LaSalle's Invariance Principle, every solution in the feasible region Ω converges to the disease-free equilibrium point as $t \to \infty$. Hence, the disease-free equilibrium E_0 is globally asymptotically stable whenever $R_0 < 1$.

Remark 3.6. *Biological Interpretation*
The global asymptotic stability of the disease-free equilibrium implies that whenever $R_0 < 1$, the infection cannot persist in the population. Consequently, the infected populations and environmental bacterial concentration gradually vanish over time, and the system converges to the disease-free steady state.

3.5.2 Global Stability of the Endemic Equilibrium

In this section, we establish the global asymptotic stability of the endemic equilibrium point using a suitable Goh–Volterra type Lyapunov function together with LaSalle's Invariance Principle. At equilibrium, the following relations hold:

$$\begin{aligned}
\Lambda + \omega_c R_c^* &= (\lambda_c^* + \phi + \mu)S_c^*, \\
\phi S_c^* + \omega_a R_a^* &= (\lambda_a^* + \mu)S_a^*, \\
\lambda_c^* S_c^* &= A_c I_c^*, \\
\lambda_a^* S_a^* &= A_a I_a^*, \\
\gamma_c I_c^* &= W_c R_c^*, \\
\gamma_a I_a^* &= W_a R_a^*, \\
\alpha_c I_c^* + \alpha_a I_a^* &= Q B^*,
\end{aligned} \tag{23}$$

where

$$A_c = \gamma_c + \delta_c + \mu, \qquad A_a = \gamma_a + \delta_a + \mu, \qquad W_c = \omega_c + \mu, \qquad W_a = \omega_a + \mu, Q = \theta + \mu_b,$$

and

$$\lambda_c^* = \beta_{cc} I_c^* + \frac{\beta_b B^*}{K + B^*}, \qquad \lambda_a^* = \beta_{aa} I_a^* + \frac{\beta_b B^*}{K + B^*}.$$

Theorem 3.7. *Suppose that $R_0 > 1$ and the endemic equilibrium point E^* exists uniquely in the feasible region Ω. Then E^* is globally asymptotically stable in Ω.*

Proof. Consider the Lyapunov function

$$V = \left(S_c - S_c^* - S_c^* \ln \frac{S_c}{S_c^*}\right) + \left(S_a - S_a^* - S_a^* \ln \frac{S_a}{S_a^*}\right) + \left(I_c - I_c^* - I_c^* \ln \frac{I_c}{I_c^*}\right) + \left(I_a - I_a^* - I_a^* \ln \frac{I_a}{I_a^*}\right) + \left(R_c - R_c^* - R_c^* \ln \frac{R_c}{R_c^*}\right) + \left(R_a - R_a^* - R_a^* \ln \frac{R_a}{R_a^*}\right) + \left(B - B^* - B^* \ln \frac{B}{B^*}\right). \tag{24}$$

Recall that for any positive number x, $x - 1 - \ln x \geq 0$. Hence, $z - z^* - z^* \ln \frac{z}{z^*} \geq 0$ for all positive z. Therefore, $V \geq 0$, with equality if and only if

$$S_c = S_c^*, \quad S_a = S_a^*, \quad I_c = I_c^*, \quad I_a = I_a^*, \quad R_c = R_c^*, \quad R_a = R_a^*, \quad B = B^*.$$

Thus, the Lyapunov function is positive definite with respect to the endemic equilibrium. Differentiating V along solutions of the system yields

$$\dot{V} = \left(1 - \frac{S_c^*}{S_c}\right)\dot{S}_c + \left(1 - \frac{S_a^*}{S_a}\right)\dot{S}_a + \left(1 - \frac{I_c^*}{I_c}\right)\dot{I}_c + \left(1 - \frac{I_a^*}{I_a}\right)\dot{I}_a + \left(1 - \frac{R_c^*}{R_c}\right)\dot{R}_c + \left(1 - \frac{R_a^*}{R_a}\right)\dot{R}_a + \left(1 - \frac{B^*}{B}\right)\dot{B}. \tag{25}$$

Substituting the model equations into $\dot{V}$ and applying the endemic equilibrium identities, after straightforward algebraic simplification we obtain

$$\dot{V} = -\lambda_c^* S_c^* \left[\frac{S_c^*}{S_c} + \frac{\lambda_c S_c I_c^*}{\lambda_c^* S_c^* I_c} + \frac{I_c}{I_c^*} - 3\right] - \lambda_a^* S_a^* \left[\frac{S_a^*}{S_a} + \frac{\lambda_a S_a I_a^*}{\lambda_a^* S_a^* I_a} + \frac{I_a}{I_a^*} - 3\right] - \gamma_c I_c^* \left[\frac{I_c}{I_c^*} + \frac{I_c^* R_c}{I_c R_c^*} - 2\right] - \gamma_a I_a^* \left[\frac{I_a}{I_a^*} + \frac{I_a^* R_a}{I_a R_a^*} - 2\right] - QB^* \left[\frac{B}{B^*} + \frac{B^*(\alpha_c I_c + \alpha_a I_a)}{B(\alpha_c I_c^* + \alpha_a I_a^*)} - 2\right]. \tag{26}$$

Now observe that each bracketed expression is non-negative by the Arithmetic Mean–Geometric Mean inequality. Indeed, for positive numbers $x_1, x_2, \ldots, x_n$,

$$\frac{x_1 + x_2 + \cdots + x_n}{n} \geq \sqrt[n]{x_1 x_2 \cdots x_n}.$$

For the first bracketed term, define $x_1 = \frac{S_c^*}{S_c}$, $x_2 = \frac{\lambda_c S_c I_c^*}{\lambda_c^* S_c^* I_c}$, $x_3 = \frac{I_c}{I_c^*}$. Then $x_1 x_2 x_3 \frac{\lambda_c}{\lambda_c^*}$.

At equilibrium, $\lambda_c = \lambda_c^*$, hence, $x_1 x_2 x_3 = 1$. Therefore, $x_1 + x_2 + x_3 \geq 3$. Similarly, all remaining bracketed expressions are non-negative. Consequently, $\dot{V} \leq 0$. Furthermore, $\dot{V} = 0$ if and only if

$$S_c = S_c^*, \quad S_a = S_a^*, \quad I_c = I_c^*, \quad I_a = I_a^*, \quad R_c = R_c^*, \quad R_a = R_a^*, \quad B = B^*.$$

Hence, the largest invariant subset contained in $\{\dot{V} = 0\}$ is the singleton set $\{E^*\}$. Therefore, by LaSalle's Invariance Principle, every solution in the feasible region Ω converges to the endemic equilibrium point E^* as $t \to \infty$. Thus, the endemic equilibrium point E^* is globally asymptotically stable whenever $R_0 > 1$.

3.6 Sensitivity Analysis of the Basic Reproduction Number

Sensitivity analysis of the basic reproduction number is carried out to determine the relative influence of the epidemiological parameters governing disease transmission and persistence. This analysis identifies the parameters that contribute most significantly to the spread of the disease and provides useful insight into effective intervention and control strategies.

3.6.1 Normalized Forward Sensitivity Index

To quantify the influence of model parameters on disease transmission, we employ the normalized forward sensitivity index. For a differentiable function $R = R(p)$, the normalized forward sensitivity index of R with respect to a parameter p is defined by

$$\Upsilon_p^R = \frac{\partial R}{\partial p} \cdot \frac{p}{R}. \tag{27}$$

The quantity Υ_p^R measures the relative change in R generated by a relative change in the parameter p.

3.6.2 Basic Reproduction Number

Recall that the basic reproduction number of the model is given by

$$R_0 = \max\{R_c, R_a\}, \tag{28}$$

where

$$R_c = \frac{\beta_{cc}\Lambda}{(\phi+\mu)(\gamma_c+\delta_c+\mu)} + \frac{\beta_b\alpha_c\Lambda}{K(\phi+\mu)(\gamma_c+\delta_c+\mu)(\theta+\mu_b)}, \tag{29}$$

and

$$R_a = \frac{\beta_{aa}\phi\Lambda}{\mu(\phi+\mu)(\gamma_a+\delta_a+\mu)} + \frac{\beta_b\alpha_a\phi\Lambda}{K\mu(\phi+\mu)(\gamma_a+\delta_a+\mu)(\theta+\mu_b)}. \tag{30}$$

Since R_0 is defined as the maximum of R_c and R_a, sensitivity analysis is performed separately for the child and adult reproduction components. This avoids the differentiability issue associated with the maximum function at the point $R_c = R_a$.

3.6.3 Sensitivity Indices of the Child Reproduction Number R_c

Using equation (29), the sensitivity indices of selected parameters are obtained as follows.

Sensitivity with respect to Λ. Since R_c depends linearly on Λ, we have

$$\frac{\partial R_c}{\partial \Lambda} = \frac{R_c}{\Lambda}.$$

Hence,

$$\Upsilon_\Lambda^{R_c} = \frac{\partial R_c}{\partial \Lambda} \cdot \frac{\Lambda}{R_c} = 1. \tag{31}$$

Sensitivity with respect to β_{cc}. Differentiating R_c with respect to β_{cc} gives

$$\frac{\partial R_c}{\partial \beta_{cc}} = \frac{\Lambda}{(\phi+\mu)(\gamma_c+\delta_c+\mu)}.$$

Therefore,

$$\Upsilon_{\beta_{cc}}^{R_c} = \frac{\beta_{cc}\Lambda}{R_c(\phi+\mu)(\gamma_c+\delta_c+\mu)} > 0. \tag{32}$$

Sensitivity with respect to γ_c. Differentiating R_c with respect to γ_c, we obtain

$$\frac{\partial R_c}{\partial \gamma_c} = -\frac{R_c}{\gamma_c+\delta_c+\mu}.$$

Consequently,

$$\Upsilon_{\gamma_c}^{R_c} = -\frac{\gamma_c}{\gamma_c+\delta_c+\mu} < 0. \tag{33}$$

Sensitivity with respect to μ_b. Differentiating R_c with respect to μ_b yields

$$\frac{\partial R_c}{\partial \mu_b} = -\frac{\beta_b\alpha_c\Lambda}{K(\phi+\mu)(\gamma_c+\delta_c+\mu)(\theta+\mu_b)^2}.$$

Thus,

$$\Upsilon_{\mu_b}^{R_c} = -\frac{\beta_b\alpha_c\Lambda\mu_b}{R_cK(\phi+\mu)(\gamma_c+\delta_c+\mu)(\theta+\mu_b)^2} < 0. \tag{34}$$

3.6.4 Sensitivity Indices of the Adult Reproduction Number R_a

Similarly, the sensitivity indices for the adult reproduction number are obtained.

Sensitivity with respect to β_{aa}.

$$\Upsilon_{\beta_{aa}}^{R_a} = \frac{\beta_{aa}\phi\Lambda}{R_a\mu(\phi+\mu)(\gamma_a+\delta_a+\mu)} > 0. \tag{35}$$

Sensitivity with respect to γ_a.

$$\Upsilon_{\gamma_a}^{R_a} = -\frac{\gamma_a}{\gamma_a+\delta_a+\mu} < 0. \tag{36}$$

Sensitivity with respect to θ.

$$\Upsilon_{\theta}^{R_a} = -\frac{\beta_b\alpha_a\phi\Lambda\theta}{R_aK\mu(\phi+\mu)(\gamma_a+\delta_a+\mu)(\theta+\mu_b)^2} < 0. \tag{37}$$

The sensitivity analysis indicates that transmission rates, bacterial shedding, and susceptible recruitment positively influence the basic reproduction number, thereby promoting disease persistence. Conversely, recovery, bacterial decay, environmental sanitation, and reduced environmental infectivity exert negative effects on R_0, contributing to disease control. From an epidemiological perspective, the results underscore the dual role of direct transmission and environmental contamination in sustaining cholera outbreaks. Therefore, effective control strategies should combine measures that reduce transmission and bacterial shedding with interventions that enhance treatment, recovery, and environmental sanitation. Such integrated approaches are essential for reducing R_0 below unity and achieving sustainable cholera elimination.

3.7 Model Fitting and Parameter Estimation

Monthly cumulative cholera case data for children and adults collected through household surveys in Shendam Local Government Area, Plateau State, Nigeria, from January to December 2025 were used to calibrate the proposed model (Table 3). Demographic parameters were estimated from population and vital statistics. Using the 2006 population census of 205,119 and an annual growth rate of 2.5%, the 2025 population was projected to be 327,914. The recruitment rate, natural mortality rate, and maturation rate were estimated from published demographic data and are summarized in Table 4. Parameter estimation was performed by fitting the model to the observed cumulative cholera cases using a nonlinear least-squares approach implemented in MATLAB. Fixed parameter values were obtained from the literature (Table 5), while key transmission and recovery parameters were estimated by minimizing the discrepancy between model predictions and observed data. The model equations were solved numerically using the `ode45` solver, and optimization was carried out using the Nelder–Mead simplex algorithm (`fminsearch`). The calibrated model provided a good fit to the data, with a coefficient of determination of $R^2 = 0.93$, indicating strong agreement between observed and simulated cholera cases. The estimated parameter values are presented in Table 6, and the corresponding model fit is shown in Figure 2.

Table 3. Monthly cumulative cholera cases used for model calibration.

Month	Children	Adults
January	2	1
February	5	3
March	9	6
April	14	9
May	21	13
June	31	19
July	44	28
August	58	38
September	70	46
October	79	52
November	85	56
December	89	59

Table 4. Demographic parameters used in the model.

Parameter	Description	Value	Source
N	Projected population of Shendam LGA (2025)	$327,914$	(NPC, 2006)
Λ	Recruitment rate	$31.8\ \text{day}^{-1}$	(World Bank, 2023)
μ	Natural mortality rate	$4.44 \times 10^{-5}\ \text{day}^{-1}$	(World Bank, 2023)
ϕ	Maturation rate	$1.83 \times 10^{-4}\ \text{day}^{-1}$	Estimated

Table 5. Fixed parameter values used in the model simulations.

Parameter	Value	Source
δ_c	0.015 day^{-1}	(Codeço, 2001; Wang, 2022)
δ_a	0.008 day^{-1}	(Codeço, 2001; Wang, 2022)
ω_c	$\frac{1}{3\times365} = 9.13 \times 10^{-4}$ day^{-1}	(Koelle et al., 2005)
ω_a	$\frac{1}{3\times365} = 9.13 \times 10^{-4}$ day^{-1}	(Koelle et al., 2005)
α_c	10 cells ml^{-1}day^{-1}	(Tuite et al., 2011; Wang, 2022)
α_a	8 cells ml^{-1}day^{-1}	(Tuite et al., 2011; Wang, 2022)
θ	$\frac{1}{30} = 0.0333$ day^{-1}	(Codeço, 2001)
μ_b	0.03 day^{-1}	(Hartley et al., 2006)
K	10^6 cells ml^{-1}	(Codeço, 2001)

Table 6. Estimated model parameters obtained from fitting the model to cholera data from Shendam Local Government Area.

Parameter	Description	Estimated value
β_{cc}	Child-to-child transmission rate	0.0030 day^{-1}
β_{aa}	Adult-to-adult transmission rate	0.0011 day^{-1}
β_b	Environmental transmission rate	0.1147 day^{-1}
γ_c	Recovery rate of children	0.1796 day^{-1}
γ_a	Recovery rate of adults	0.2158 day^{-1}

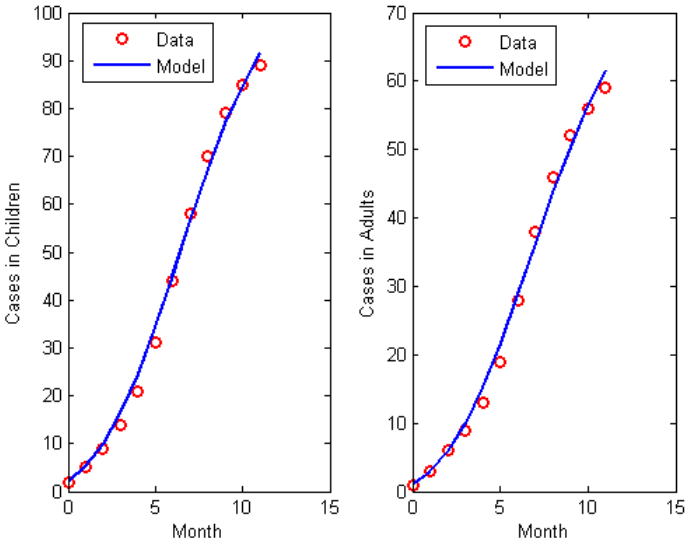

Figure 2. Comparison between observed cumulative cholera cases and model predictions for children and adults in Shendam Local Government Area. Circles represent observed data, while solid curves denote model simulations obtained using the estimated parameter values.

3.8 Numerical Simulations

Numerical simulations were carried out in MATLAB using the `ode45` solver. The parameter values employed in the simulations are summarized in Tables 4, 5, and 6 . In the first set of simulations, the effect of environmental hygiene on cholera transmission was

investigated using the infected child and adult populations as indicators of disease burden. The simulation results show that an increase in the level of environmental hygiene leads to a significant reduction in the number of infected individuals among both children and adults, as illustrated in Figure 3. This finding suggests that improved environmental hygiene is an effective control strategy for reducing cholera transmission in Shendam Local Government Area of Plateau State, Nigeria. The results further emphasize the importance of access to safe water, proper sanitation, and effective waste management in mitigating cholera outbreaks.

In the second set of simulations, the impact of treatment, represented through the recovery rates of infected individuals, was examined. The results indicate that increasing the treatment rates leads to a corresponding increase in the number of recovered individuals in both the child and adult populations, as shown in Figure 4. This outcome demonstrates the critical role of timely diagnosis and effective treatment in controlling cholera outbreaks. Enhanced treatment coverage not only improves recovery outcomes but also reduces the duration of infectiousness, thereby contributing to a reduction in disease transmission within the community.

Overall, the simulation results highlight the combined importance of environmental hygiene and effective treatment interventions in reducing the burden of cholera. Consequently, public health policies aimed at improving sanitation infrastructure, ensuring access to clean water, and strengthening healthcare services are essential for the effective control and prevention of cholera in Shendam Local Government Area and similar endemic settings.

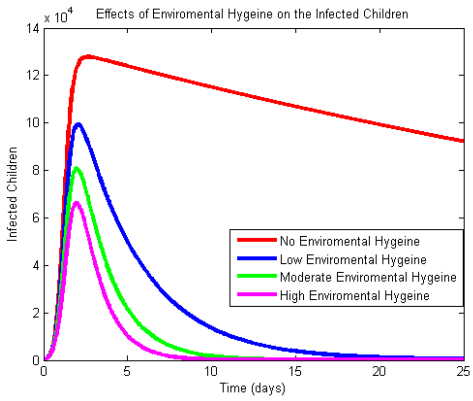

(a) Effects of Environmental Hygiene on the Infected Children

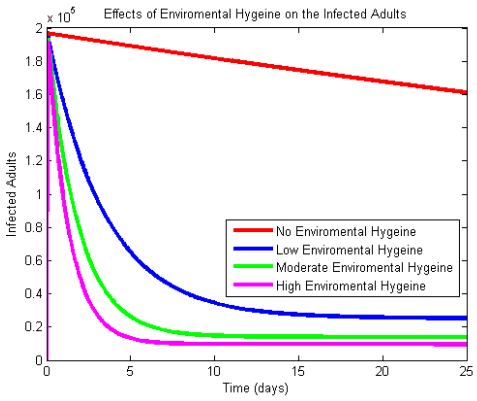

(b) Effects of Environmental Hygiene on the Infected Adults

Figure 3. Effects of Environmental Hygiene on the Transmission Dynamics of Cholera.

4 Results

4.1 Mathematical Analysis

The proposed cholera model was shown to be mathematically and epidemiologically well posed, with all solutions remaining nonnegative and bounded within a biologically feasible region. The disease-free equilibrium (DFE) and the basic reproduction number, R_0, were derived using the next-generation matrix approach. Stability analysis established that

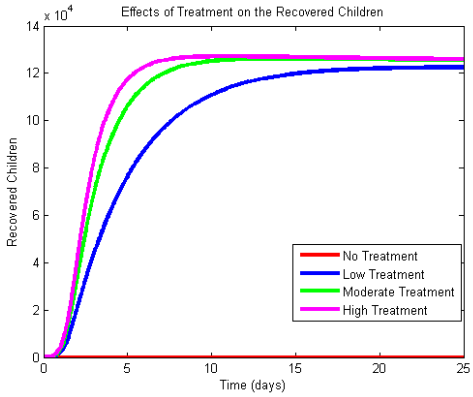

(a) Effects of Treatment on the Recovered Children

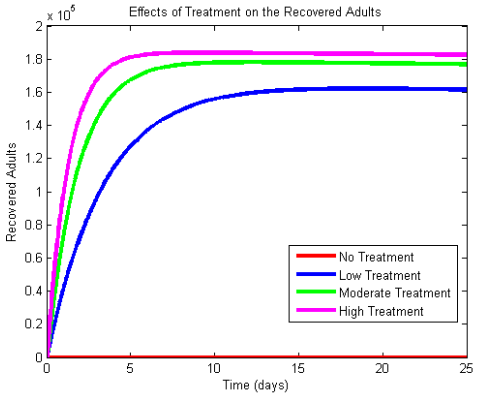

(b) Effects of Treatment on the Recovered Adults

Figure 4. Effects of Treatment on the Transmission Dynamics of Cholera.

the DFE is globally asymptotically stable when $R_0 < 1$, implying disease elimination. In contrast, a unique endemic equilibrium exists and is globally asymptotically stable whenever $R_0 > 1$, indicating sustained cholera transmission.

4.2 Model Fitting and Parameter Estimation

The model was calibrated using cumulative cholera case data collected in Shendam Local Government Area between January and December 2025. The estimated parameters are presented in Table 6, while the fitted trajectories are shown in Figure 2. The model reproduced the observed cholera dynamics with good accuracy, demonstrating its suitability for describing disease transmission within the study population.

4.3 Sensitivity Analysis

Sensitivity analysis revealed that transmission rates, bacterial shedding rates, and recruitment rate exert the strongest positive influence on R_0, thereby promoting disease persistence. Conversely, recovery rates, bacterial decay, sanitation, disease-induced mortality, and reduced environmental infectivity negatively affect R_0, highlighting their importance in disease control.

4.4 Numerical Simulations

Numerical simulations demonstrated that improvements in environmental hygiene significantly reduce infection prevalence among both children and adults, while enhanced treatment increases recovery and shortens the infectious period. Overall, the results suggest that integrated interventions combining environmental sanitation and effective treatment can substantially reduce cholera transmission and disease burden.

5 Discussion

The results demonstrate that the proposed cholera model is biologically and epidemiologically well posed, with all state variables remaining positive and bounded within a feasible region. The basic reproduction number, R_0, was identified as the key threshold parameter governing disease dynamics. The global asymptotic stability of the disease-free equilibrium when $R_0 < 1$ indicates that cholera can be eliminated if control measures

successfully reduce transmission below the epidemic threshold. Conversely, the global asymptotic stability of the endemic equilibrium when $R_0 > 1$ confirms that cholera persists in the population whenever transmission remains sufficiently high.

Model calibration showed good agreement between observed and simulated cholera cases in Shendam Local Government Area, demonstrating the ability of the model to capture the underlying transmission dynamics. The findings further emphasize the importance of incorporating both age structure and environmental contamination in understanding cholera spread.

Sensitivity analysis revealed that transmission-related parameters, including direct human-to-human transmission, environmental exposure, and bacterial shedding, exert the greatest influence on disease transmission. In contrast, recovery and environmental sanitation were found to reduce disease burden by lowering the effective reproduction number. These observations are consistent with previous studies that identify contaminated water sources and environmental reservoirs as major drivers of cholera outbreaks.

Numerical simulations further supported the analytical results by showing that improved environmental hygiene significantly reduces infection prevalence through decreased bacterial contamination, while increased treatment rates enhance recovery and shorten the infectious period. Overall, the results indicate that sustainable cholera control requires integrated interventions targeting both human transmission pathways and environmental reservoirs to effectively reduce transmission and achieve long-term disease elimination.

6 Conclusion

This study developed and analyzed an age-structured cholera transmission model that incorporates environmental contamination and was calibrated using cholera data from Shendam Local Government Area, Plateau State, Nigeria. The model was shown to be mathematically and epidemiologically well posed, and the basic reproduction number, R_0, was derived as the key threshold parameter governing disease dynamics.

Theoretical results established that cholera can be eliminated when $R_0 < 1$, whereas persistent transmission occurs when $R_0 > 1$. Model calibration demonstrated good agreement between observed and simulated data, confirming the model's ability to capture the transmission dynamics of cholera in the study area. Sensitivity analysis identified transmission and bacterial shedding parameters as the most influential drivers of disease persistence, while recovery, bacterial decay, and environmental sanitation contribute to disease reduction.

Numerical simulations further revealed that improvements in environmental hygiene and treatment coverage significantly reduce infection prevalence and disease burden. Overall, the findings highlight the importance of integrated control strategies combining sanitation, safe water provision, environmental management, rapid diagnosis, and effective treatment to reduce transmission, prevent endemic persistence, and support the long-term elimination of cholera in endemic communities.

Ethics Approval and Informed Consent

Ethical approval was not required for this study. Informed consent was obtained from all participants.

Conflicts of Interest

The authors declare no conflict of interest.

Acknowledgements

The authors gratefully acknowledge the Tertiary Education Trust Fund (TETFund), Nigeria, for funding this research through the Institution-Based Research (IBR) intervention. We also express our sincere appreciation to the Management of Federal Polytechnic N'yak-Shendam, Plateau State, Nigeria, for their encouragement, support, and provision of a conducive environment for this research.

References

Abubakar, A. T.; Dalhat, M., and Nguku, P. (2016). Cholera outbreak - IDP camps in Maiduguri, northern Nigeria. *International Journal of Infectious Diseases*, **45**, *132*. https://doi.org/10.1016/j.ijid.2016.02.326

Adejoro, L. (2025). Cholera, Lassa fever, others killed 1,738 in 2025. The Punch. https://punchng.com/cholera-lassa-fever-others-killed-1738-in-2025/

Africa Centres for Disease Control and Prevention. (2025). Continental cholera preparedness and response plan for Africa 1.0. Africa CDC.

Ali, M.; Nelson, A.R.; Lopez, A.L.; and Sack, D.A (2015) Updated Global Burden of Cholera in Endemic Countries. *PLoS Negl Trop Dis* **9**(6): e0003832. https://doi.org/10.1371/journal.pntd.0003832

Anderson, R. M., and May, R. M. (1991). *Infectious diseases of humans: Dynamics and control*. Oxford University Press.

Brauer, F., Shuai, Z., and Van den Driessche, P. (2013). Dynamics of an age-of-infection cholera model. *Mathematical Biosciences and Engineering*, (5/6), 1335–1359. https://doi.org/10.3934/mbe.2013.10.1335

Granas, A., & Dugundji, J.(2003). *Fixed point theory*. New York, NY: Springer. https://doi.org/10.1007/978-0-387-21593-8

Cai, L.; Modnak, C.; and Wang, J. (2017). An age-structured model for cholera control with vaccination. *Applied Mathematics and Computation*, **299**, 127—140. https://doi.org/10.1016/j.amc.2016.11.013

Cai, L.; Fan, G.; Yang, C.; and Wang, J. (2020). Modeling and analyzing cholera transmission dynamics with vaccination age. *Journal of the Franklin Institute*, **357**(12), 8008–8034.https://doi.org/10.1016/j.jfranklin.2020.05.030

Cheng, X.; Wang, Y.; & Huang, G. (2024). Dynamical analysis of an age-structured cholera transmission model on complex networks. *Journal of Mathematical Analysis and Applications*, **531**(2), 127833. https://doi.org/10.1016/j.jmaa.2023.127833

Cheng, X., Wang, Y., and Huang, G. (2023). Dynamics of cholera transmission model with imperfect vaccination and demographics on complex networks. *Journal of the*

Franklin Institute, **360**(2), 1077—1105. https://doi.org/10.1016/j.jfranklin.2022.12.006

Codeço, C. T. (2001). Endemic and epidemic dynamics of cholera: The role of the aquatic reservoir. *BMC Infectious Diseases*, **1**(1), 1. https://doi.org/10.1186/1471-2334-1-1

Diekmann, O.; Heesterbeek, J. A. P.; and Roberts, M. G. (2010). The construction of next-generation matrices for compartmental epidemic models. *Journal of the Royal Society Interface*, **7**(47), 873–885. https://doi.org/10.1098/rsif.2009.0386

Driessche V. & Watmough J. (2002). Reproduction numbers and sub-threshold endemic equilibria for compartmental models of disease transmission.*Math Biosci*, 2002;180:29–48 .

Finger, F.; Bertuzzo, E.; Luquero, F.J.; Naibei, N.; Touré, B.; Allan, M.; Porten, K.; Lessler, J.; Rinaldo, A.; and Azman, A.S. (2018). The potential impact of case-area targeted interventions in response to cholera outbreaks: A modeling study. *PLoS Med.***15**(2):e1002509. doi:10.1371/journal.pmed.1002509.PMID:29485987;PMCID:PMC5828347.

Hartley, D. M.; Morris, J. G.; and Smith, D. L. (2006). Hyperinfectivity: A critical element in the ability of Vibrio cholerae to cause epidemics? *PLoS Medicine*, **3**(1), https://doi.org/10.1371/journal.pmed.0030007

Heesterbeek, H.; Anderson, R. M.; Andreasen, V.; Bansal, S.; De Angelis, D.; Dye, C.; Eames, K. T. D.; Edmunds, W. J.; Frost, S. D. W.; Funk, S.; Hollingsworth, T. D.; House, T.; Isham, V.; Klepac, P.; Lessler, J.; Lloyd-Smith, J. O.; Metcalf, C. J. E.; Mollison, D.; Pellis, L.; and Yates, C. A. (2015). Modeling infectious disease dynamics in the complex landscape of global health. *Science*, **347**(6227), aaa4339. https://doi.org/10.1126/science.aaa4339

Hethcote, H. W. (2000). The mathematics of infectious diseases.*SIAM Review*, **42**(4), 599—653. https://doi.org/10.1137/S0036144500371907

Hove-Musekwa, S. D.; Nyabadza, F.; Chiyaka, C.; Das, P.; Tripathi, A., and Mukandavire, Z. (2011). Modelling and analysis of the effects of malnutrition in the spread of cholera. *Mathematical and Computer Modelling*, **53**(9-10), 1583–1595. https://doi.org/10.1016/j.mcm.2010.11.060

Keeling, M. J., and Rohani, P. (2008). *Modeling infectious diseases in humans and animals*. Princeton University Press.

Koelle, K., Rodó, X., Pascual, M., Yunus, M., & Mostafa, G. (2005). Refractory periods and climate forcing in cholera dynamics.*Nature, 436*(7051), 696–700. https://doi.org/10.1038/nature03820

Lin, J.; Xu, R.; and Tian, X. (2019). Global dynamics of an age-structured cholera model with multiple transmissions, saturation incidence and imperfect vaccination. *Journal of Biological Dynamics*, **13**(1), 69-–102.https://doi.org/10.1080/17513758.2019.1570362

Lakshmikantham, V.; and Leela, S. (1969). *Differential and integral inequalities: Theory and applications: Vol. 2. Functional, partial, abstract, and complex differential equations*. Academic Press.

Mossong, J.; Hens, N.; Jit, M.; Beutels, P.; Auranen, K.; Mikolajczyk, R.; Massari, M.; Salmaso, S.; Tomba, G. S.; Wallinga, J.; Heijne, J.; and Sadkowska-Todys, M. (2008). Social contacts and mixing patterns relevant to the spread of

infectious diseases. *PLoS Medicine*, **5**(3), e74.https://doi.org/10.1371/journal.pmed.0050074

Mukandavire, Z., Liao, S., Wang, J., Gaff, H., Smith, D. L., and Morris, J. G. (2011). Estimating the reproductive numbers for the 2008–2009 cholera outbreaks in Zimbabwe. *Proceedings of the National Academy of Sciences*, **108**(21), 8767-–8772. https://doi.org/10.1073/pnas.1019712108

Mwasa, A., & Tchuenche, J. M. (2011). Mathematical analysis of a cholera model with public health interventions. *Biosystems*, **105**(3), 190—200.

Nigeria Centre for Disease Control. (2020). National cholera emergency operations centre situation report.

National Population Commission (NPC). (2006). *2006 Population and Housing Census of the Federal Republic of Nigeria: National and State Population and Housing Tables.* Abuja, Nigeria: National Population Commission.

Sun, G.Q., Xie, J.-H., Huang, S.-H., Jin, Z., Li, M.-T., & Liu, L. (2017). Transmission dynamics of cholera: Mathematical modeling and control strategies. *Communications in Nonlinear Science and Numerical Simulation*, **45**, 235–244. https://doi.org/10.1016/j.cnsns.2016.10.007

United Nations Children's Fund. (2025, May). Nigeria flash report. UNICEF Nigeria. https://www.unicef.org/nigeria/reports/nigeria-flash-report

Tien, J. H., & Earn, D. J. D. (2010). Multiple transmission pathways and disease dynamics in a waterborne pathogen model. *Bulletin of Mathematical Biology*, **72**(6), 1506–1533. https://doi.org/10.1007/s11538-010-9507-6

Tuite, A. R., Tien, J., Eisenberg, M., Earn, D. J. D., Ma, J., & Fisman, D. N. (2011). Cholera epidemic in Haiti, 2010: Using a transmission model to explain spatial spread of disease and identify optimal control interventions. *Annals of Internal Medicine, 154*(9), 593–601. https://doi.org/10.7326/0003-4819-154-9-201105030-00334

Wallinga, J., Teunis, P., and Kretzschmar, M. (2006). Using data on social contacts to estimate age-specific transmission parameters for respiratory-spread infectious agents. *American Journal of Epidemiology*, 1**64**(10), 936–944. https://doi.org/10.1093/aje/kwj317

Wang, J. (2022). Mathematical models for cholera dynamics—A review.*Microorganisms, 10*(12), 23–58. https://doi.org/10.3390/microorganisms10122358

World Health Organization (2022). Cholera fact sheet. Geneva:

World Health Organization. (2024a, December 5). Cholera.

World Health Organization. (2024b, February 12). Multi-country outbreak of cholera: External situation report.

World Health Organization (2023). Multi-country outbreak of cholera: Situation report.

World Health Organization (WHO). (2024, May 4). Weekly Epidemiological Record: Cholera, 2024. Geneva: WHO.

World Health Organization. (2026, January 27). Multi-country outbreak of cholera: Epidemiological update.

World Bank. (2023). *Birth rate, crude (per 1,000 people) – Nigeria.* World Development Indicators. Retrieved from https://data.worldbank.org/indicator/SP.DYN.CBRT.IN

World Bank. (2023). *Life expectancy at birth, total (years) – Nigeria.* World Development

Indicators. Retrieved from https://data.worldbank.org/indicator/SP.DYN.LE00.IN

Yang, D.; Zhipeng, Q.; Xue-Zhi, L. (2014). Global stability of an age-structured cholera model *Mathematical Biosciences and Engineering*, **11**(3): 641–665. https://doi.org/10.3934/mbe.2014.11.641